공학석사학위논문

사람 손 움직임을 반영한 부족구동 텐던구동 로봇 손의 디자인 및 제어

Design and Control of Under-Actuated Tendon-Driven Robotic Hand Reflecting Human Hand Motion Analysis

2017 년 2 월

서울대학교 대학원

기계항공공학부

김 주 혁

Abstract

Design and Control of Under-Actuated Tendon-Driven Robotic Hand Reflecting Human Hand Motion Analysis

Juhyeok Kim
Mechanical & Aerospace Engineering
The Graduate School
Seoul National University

We propose a novel design framework for the under-actuated tendon-driven (UATD) robotic finger. In this study, we decompose the system equation based on its stiffness to separate the "actuated" space and the "un-actuated" space. The actuated space appears during the free motion when no disturbance is exerted, whereas the un-actuated space is observed when there is contact. We measure the index finger joint angles and contact force during both the free motion and the contact, and search for the efficient design parameters (stiffness, active tendon routing, initial configuration) to mimic the human finger motion. We formulate the optimization problem to find those parameters and we consider the system constraints, s.t. finger thickness and unilaterality of tendon-driven mechanism, simultaneously. We also design a simple PD-based control to track the desired joint angle, and we show the simulation results.

Keywords: Under-actuated tendon-driven robotic finger, Stiffness decomposition

Student Number: *2014-21870*

Contents

List of Figures

List of Tables

Abbreviations

UATD	**U**nder-**A**ctuated **T**endon-**D**riven
DoF	**D**egree **o**f **F**reedom
PCA	**P**rincipal **C**omponent **A**nalysis
MCP	**M**eta**C**arpo**P**halangeal joint
PIP	**P**roximal **I**nter**P**halangeal joint
DIP	**D**istal **I**nter**P**halangeal joint
PP	**P**roximal **P**halanx
MP	**M**iddle **P**halanx
DP	**D**istal **P**halanx

Chapter 1

Introduction

Human hand is regarded as one of the most dexterous system in the nature. It has many bones, intrinsic muscles and tendons of extrinsic muscles. They generate 27 D.O.F. motions, which enable hands to perform complex task, s.t. power grip, precision grip, in-hand manipulation. Due to this dexterity, many researches have studied to design a robotic hand mimicking the human hand. Especially, tendon-driven mechanism have been widely used for the actuation due to its distinct advantages [1]-[7]. We can reduce the inertia of the fingers by locating relatively heavy actuators remotely, generate joint coupling and allocate the active directions by adjusting the tendon routing and the pulley radii [8]. Also, under-actuation have been used to reduce the number of actuators and system complexity. In the human hand, due to its anatomical structure, some joints can not move independently. Especially, the proximal interphalangeal joint (PIP) and

the distal interphalangeal joint (DIP) are coupled [9], and some researches use this in their robotic hands [10, 11].

Several studies have handled the design problem for the anthropomorphic robotic hand to mimic the human hand [10]-[18]. Some studied how to determine the tendon routing, joint pulley radii to maximize the grasp quality under the constraints [12]-[14]. They first defined the grasp quality based on the feasible object wrench during the grasping the pre-determined object and search for optimal design parameter set. They include the system constraints like maximum pulley radii from the human hand and maximal tendon tensions. However, they treat only fully actuated robotic hands, so their approach can not be applied to the under-actuated system having un-actuated direction, which can not resist the external wrench.

For under-actuated hand, there have been several researches to mimic the free motion of human hand [10, 11, 15]. However, they focused on realization of free motion and did not consider the contact during task. This leads to different postures when the external force is exerted. Some researches used synergies to reduce the number of actuators for performing tasks [16]-[18]. They selected some major motions and applied the principal component analysis (PCA) to find the distribution of actuation. They treat the free motion, so they have same shortcoming. Also, they used a motion for specific task, their design can not cover the all possible workspace.

In this study, we propose general design framework for the under-actuated tendon-driven (UATD) robotic finger based on novel stiffness decomposition. In particular, we aim to realize a UATD robotic finger, which mimics human index finger both during free motion and pinch pushing (pushing for pinch grip), even with under-actuation and passive compliance. For this, we propose the stiffness decomposition, which splits the total stiffness (i.e., with both passive and active compliances) into the two following spaces: 1) the"actuated" space, in which the behavior of the robotic finger becomes fully-actuated, thus, can be arbitrarily controlled; and 2) the "un-actuated" space, in which the effect of actuation vanishes, thus, the finger control should purely rely on the passive compliance of the UATD finger.

Using this stiffness decomposition, we first perform the free motion analysis of the human index finger, extract the major components of the target motion via PCA similar to the case of motion synergy, and determine the actuated space. Then, we define the passie elements (e.g. passive tendon routing and torsional spring) by minimizing the deformation in the un-actuated direction. This enables the robotic finger to resist the large contact force for some human-like configurations. With this stiffness from passive elements, we determine the active tendon routing and initial configuration to cover the actuated space under the system constraints. We also propose a simple PD-based control scheme for this UATD robotic finger and verify the results by simulation.

Chapter 2

Preliminary

2.1 Modeling of UATD Robotic Finger

The UATD robotic finger has active and passive tendons, where the active tendon is directly connected to an actuator (e.g., motor), while the passive tendon to some passive compliant elements (e.g., spring). We assume that, with some proper pre-tension, there is no slack occurs between the tendons and their pulleys throughout the routing. Then, we can obtain the following kinematic relations:

$$l_a - l_{a_o} - R_{\theta_a}(\theta_a - \theta_{a_o}) = J_{\theta_a}(q - q_o) \tag{2.1}$$

$$l_p - l_{p_o} + (\theta_p - \theta_{p_o}) = J_{\theta_p}(q - q_o) \tag{2.2}$$

where $q \in \mathcal{Q} \approx \Re^n$ is the finger configuration, $l_a \in \Re^{m_a}, l_p \in \Re^{m_p}$ are the lengths of the m_a-active and m_p-passive tendons from their reference lengths $l_{a_o} \in \Re^{m_a}$ and $l_{p_o} \in \Re^{m_p}$, $\theta_a \in \Re^{m_a}$ is the actuator motor angle with $R_{\theta_a} = diag[r_{\theta_{a_1}}, r_{\theta_{a_2}}, ...r_{\theta_{m_a}}] \in \Re^{m_a \times m_a}$ being their actuation pulley radii, $\theta_p \in \Re^{m_p}$ is the equivalent deformation of the active and passive compliant elements apparent to each passive tendon, and $J_{\theta_a} \in \Re^{m_p \times n}, J_{\theta_p} \in \Re^{m_p \times n}$ are the active and passive tendon Jacobians, capturing the pulley radii and routing of each tendon. Here, we assume $m_a < n$, i.e., the robotic finger is under-actuated. We also assume the ranks of $J_{\theta_a}, J_{\theta_p}$ be maximal.

Following [10], we also assume both the active and passive tendons be stiff, i.e., $(l_a - l_{a_o}, l_p - l_{p_o}) \approx 0$. Then, for the active tendon, we have

$$J_{\theta_a}(q - q_o) = -R_{\theta_a}(\theta_a - \theta_{a_o}) \tag{2.3}$$

that is, the joint motion q is allowed for by the change of the actuator angles θ_q under the condition that the active tendon length is constant (i.e., $l_a - l_{a_o} = 0$). Also, with the assumption that the tendon force transmission loss through the pulleys is negligible, we can further have

$$f_{\theta_a} = R_a^{-1}\tau_a \tag{2.4}$$

where $f_a \in \Re^{m_a}$ is the force of the active tendon, and $\tau_a \in \Re^{m_a}$ is the actuator torque input. Similarly, for the passive tendon, we have

$$\theta_p - \theta_{p_o} = J_{\theta_p}(q - q_o)$$

and, further, if we denote the effective stiffness of the passive compliant elements by $K_{\theta_p} \in \Re^{m_p \times m_p}$, we can compute the passive tendon force s.t.,

$$f_{\theta_p} = -K_{\theta_p}(\theta_p - \theta_{p_o}) = -K_{\theta_p} J_{\theta_p}(q - q_o)$$

Then, the joint torque $\tau \in \Re^n$ produced by the tendon actuation and passive tendon compliance for the robotic finger can be written by:

$$\tau = \begin{bmatrix} J_{\theta_a}^T & J_{\theta_p}^T \end{bmatrix} \begin{pmatrix} f_{\theta_a} \\ f_{\theta_p} \end{pmatrix} = -J_a^T \tau_a - K_p(q - q_0) \tag{2.5}$$

where $J_a := R_{\theta_a}^{-1} J_{\theta_a} \in \Re^{m_a \times n}$ and $K_p := J_{\theta_p}^T K_{\theta_p} J_{\theta_p} \in \Re^{m_p \times m_p}$. Note that the tension of the passive compliant elements $K_p(q - q_0)$ and the positive control input of the active tendon actuator τ_a are along the same direction to reduce $||q - q_o||$. Note also that J_a, K in (2.5) are all constant matrices, since so are $J_{\theta_a}, J_{\theta_p}, R_{\theta_a}$ and K_{θ_p}.

In addition to the compliance K of the passive tendons, we also assume the robotic finger is equipped with some torsional springs at some joints with their actions represented by $K_q(q - q_o)$, where $K_q \in \Re^{n \times n}$ is positive semi-definite.

Then, we can write the dynamics of the UATD robotic finger s.t.,

$$M(q)\ddot{q} + C(q,\dot{q})\dot{q} + K(q - q_0) \\ = -J_a^T \tau_a + \sum_{j \in \{\mathcal{C}\}} G_j^T(q) F_j \tag{2.6}$$

where $K := K_q + K \in \Re^{n \times n}$ and $F_j \in \Re^3$ is the j-th external force acting on a part of the robotic finger with tis contact Jacobian defined by $G_j(q) \in \Re^{n \times 3}$.

Following [10], we assume the total stiffness matrix K is positive definite, i.e., even with no actuation, the configuration of the robot finger is not undetermined. Similar assumption was made in. Also, although our proposed scheme can be easily extended, for simplicity, here, we assume each contact produces only force, not moment. Further, in this paper, we assume the dynamics effect of the robotic finger is negligible, as the inertia and the operation speed of the robotic finger is typically rather small. This quasi-static modeling can then be easily obtained from (2.6) s.t.,

$$q = q_o - K^{-1} \left[J_a^T \tau_a - \sum G_j^T(q) F_j \right] \tag{2.7}$$

with $||M(q)\ddot{q} + C(q,\dot{q})\dot{q}|| \approx 0$. This quasi-static equation (2.7) is the basis of our ensuing development and investigation in the following sections.

2.2 Design Objective

Our goal here is to design the UATD robotic finger, which mimics the human index finger behavior during the free motion and also the pinching pushing, where the contact can be approximated by a contact force, whose contact point is fixed, yet, its direction and magnitude can be varied within a certain range. For this, without loss of generality, we also set $\theta_{a_o} = 0$. Then, the quasi-static forced kinematic equation (2.7) can be reduced s.t.,

$$q - q_0 = -K^{-1}\left[J_a^T \tau_a - G^T(q)F\right] \tag{2.8}$$

where $G(q) \in \Re^{n\times 3}$ is only a function of q with the contact point predetermined at the finger tip, whereas the contact force $F \in \Re^3$ is in a certain contact force set $\mathcal{F}$, i.e., $F \in \mathcal{F}$.

We treat only the flexion/extension movement of an index finger. The abduction/adduction movement occurs at only metacarpophalangeal joint (MCP) and its direction is orthogonal to flexion/extension. We can easily make this movement with the independent mechanism, so we ignore that in this design procedure. Also, this design framework can be applied to other digits similarly, so we treat only index finger to explain process. Then, the design parameters to choose for mimicking human index finger behavior are then $K = K_q + J_{\theta_p} K_{\theta_p} J_{\theta_p}^T$ (i.e., joint torsional springs, routing configuration and pulley radii of passive tendons, and stiffness of of passive compliance elements of passive tendons), $J_a = R_{\theta_a}^{-1} J_{\theta_a}$

(i.e., routing configuration and pulley radii of active tendons), q_0 (i.e., initial configuration when actuation input τ_a is zero). Here, we assume $G(q)$ is given as the lengths of human index finger phalanges, with the range of F also pre-specified from the human subject test during the pinching pushing task. We now embark to develop this design framework for the anthropomorphic UATD robotic finger in Sec. 3, for which the novel stiffness decomposition of Sec. 3.1 turns out to be crucial.

Chapter 3

Design of UTAD Robotic Finger

3.1 Stiffness Decomposition

Consider the quasi-static forced kinematic equation of the UATD robotic finger (2.8). There, $\tau_a \in \Re^{m_a}$ can be arbitrarily assignable, which is propagated to the robot configuration through the m_a-columns of $K^{-1}J_a^T \in \Re^{n\times m_a}$, with $m_a < n$ (i.e., under-actuated). On the other hand, there would exist $(n-m_a)$-dimensional "un-actuated directions", which cannot be controlled by τ_a. We then split the configuration space $\mathcal{Q}$ of the robotic finger q of (2.8) into the m_a-dimensional "actuated" space $\mathcal{Q}_a \approx \Re^{m_a}$ and the $(n-m_a)$-dimensional "un-actuated" space

$\mathcal{Q}_u \approx \Re^{n-m_a}$ by utilizing the K-metric, i.e.,

$$\mathcal{Q} = \mathcal{Q}_a \oplus_K \mathcal{Q}_u$$

which can be written by

$$q - q_0 = \underbrace{\begin{bmatrix} K^{-1}J_a^T & N_a \end{bmatrix}}_{=:S' \in \Re^{n\times n}} \begin{pmatrix} \xi_a \\ \xi_u \end{pmatrix} \tag{3.1}$$

where $N_a \in \Re^{n\times(n-m_a)}$ is defined by

$$\left[K^{-1}J_a^T\right]^T \cdot K \cdot N_a = J_a \cdot N_a = 0$$

that is, the orthogonal complement of the actuated space $K^{-1}J_a^T$ w.r.t, the stiffness matrix K, which is also the the null-space of J_a. The component of q in the actuated space $\mathcal{Q}_a$ and un-actuated space $\mathcal{Q}_u$ are then respectively specified by $\xi_a \in \Re^{n\times m_a}$ and $\xi_u \in \Re^{n\times(n-m_a)}$.

Since $S' \in \Re^{n\times n}$ is a constant and also invertible (with K being positive definite) matrix, the coordinate transformation (3.1) is integrable with ξ_a, ξ_u representing well-defined configurations, each a linear sum of the components of $q = [q_1; q_2; ...q_n]$. Further, by multiplying both sides of (3.1) with (2.3), we can have

$$J_a(q - q_0) = J_a K^{-1} J_a^T \xi_a = -\theta_a$$

from which we obtain

$$\xi_a = -K_a \theta_a \tag{3.2}$$

where $K_a := (J_a K^{-1} J_a^T)^{-1}$ and we use $J_a = R_{\theta_a}^{-1} J_{\theta_a}$. This then means that $\xi_a \in \Re^m$ specified the motion of the robot finger q generated by the active tendon θ_a propagated through the finger compliance K^{-1}. This also means that the actuated motion space $\mathcal{Q}_a$ can be explicitly parameterized by the $\theta_a \in \Re^{m_a}$.

We can then rewrite the decomposition (3.1) s.t.,

$$q - q_0 = \underbrace{\begin{bmatrix} -K^{-1} J_a^T \cdot K_a & N_a \end{bmatrix}}_{=:S \in \Re^{n \times n}} \begin{pmatrix} \theta_a \\ \xi_u \end{pmatrix} \tag{3.3}$$

and, if we apply this transformation (3.3) to (2.8) s.t.,

$$S^T K S \begin{pmatrix} \theta_a \\ \xi_u \end{pmatrix} = -S^T [J_a^T \tau_a - G(q) F]$$

we can obtain the following decomposed quasi-static equation:

$$\begin{bmatrix} K_a & 0 \\ 0 & K_u \end{bmatrix} \begin{pmatrix} \theta_a \\ \xi_u \end{pmatrix} = \begin{pmatrix} \tau_a - K_a J_a K^{-1} G(q) F \\ N_a^T G(q) F \end{pmatrix} \tag{3.4}$$

where $K_a = (J_a K^{-1} J_a^T)^{-1}$ and $K_u := N_a^T K N_a$. Note that the first equation of (3.4) represents the robotic finger motion in the actuated space $\mathcal{Q}_a$, which can

be fully controlled by τ_a. More precisely, combining (3.3) and (3.4), we have

$$q_a = -K^{-1}J_a^T[\tau_a - K_a J_a K^{-1} G(q)F] \in \mathcal{Q}_a$$

which is the component of the robot finger motion q in the actuated space $\mathcal{Q}_a$, similarly, we also have

$$q_u = N_a K_u^{-1} N_a^T G(q)F \in \mathcal{Q}_u$$

which is the component of q in the un-actuated space $\mathcal{Q}_u$ with $q = q_0 + q_u + q_a$. With the stiffness decomposition, we can also split the design problem of UATD robotic finger into three subproblems, namely, 1) search for the joint angle space, which is range space of $K^{-1}J_a^T = (K_q + K_p)J_{\theta_a}^T R_{\theta_a}^{-1}$, to define the actuated and the unactuated space during the free motion (Sec. 3.2); 2) to minimize the deformation q_u in the un-actuated space $\mathcal{Q}_u$ given $G(q)F$ so that, during the pinching pushing, the robotic finger can maintain its posture similar to that of the human index finger without excessive bending of the fingers (Sec. 3.3); 3) to investigate the active tendon routing $J_a = R_\theta^{-1} J_{\theta_a}$, particularly, the routing configuration and pulley radii of active tendons, and the initial configuration q_0 so that the robotic finger can follow the human index finger behavior efficiently during free motion despite the unilaterality of tendon-driven actuation (Sec. 3.4).

3.2 Actuated Space Search via Motion Analysis

Here, we describe how to design a 3 DoF UATD robotic finger to mimic an actual index finger motion. Some researches have investiged the PIP-DIP coupling [9, 19] and used this in their model to reduce the complexity [20, 21]. By measuring the joint angles, we find the actuated space and the unactuated space coming from this coupling.

3.2.1 Experiments for Joint Angles

To find the actuated space and the unactuated space, we measure MCP, PIP, DIP joint angles of an index finger during free motion. Since we have no information of joint positions and their axes, we can not measure the joint angles directly. Therefore, we attached markers to the dorsum of hand, proximal phalanx (PP), middle phalanx (MP), distal phalanx (DP) as shown in Fig. 3.1.

We use the Optitrack motion capture system. The subject freely moves an index finger without any disturbance for about 66s and the frequency is 1000Hz, so the total number of data is 66307. Then, we calculate the joint positions and axes with position and orientation measurements of each body. For each joint, the optimization problem to find them [22, 23] is

$$f(c_1, c_2) = \sum_{i=1}^{N} \|(R_{i,1}c_1 + d_{i,1}) - (R_{i,2}c_2 + d_{i,2})\| \tag{3.5}$$

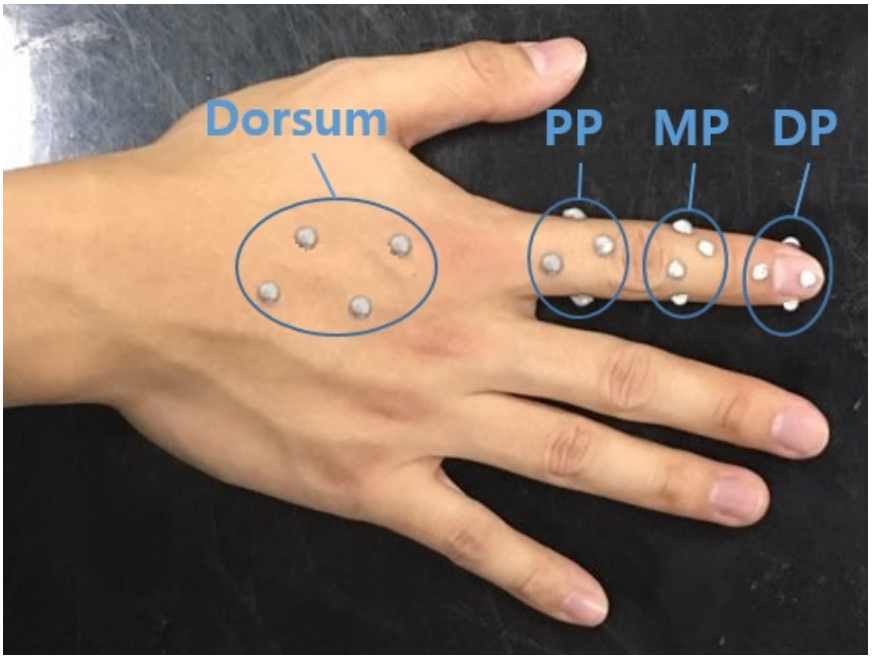

FIGURE 3.1: Experimental settings for the joint angles

where i is the order of data, N is the number of total data, $R_{i,1}, R_{i,2} \in \Re^{3\times3}$ are the rotation matrix of distal and proximal bodies, $c_1, c_2 \in \Re^3$ are the corresponding joint position in each body frame, and $d_{i,1}$, $d_{i,2}$ are the position of each body in the inertial frame. This object function f in (3.5) comes from kinematics for 1 DoF joint, s.t. the joint position calculated from distal and proximal bodies should be same. Ideally, the optimal value becomes zero, but due to the measurement error and the minor movements of joint, especially for MCP, it is

not. Then, the optimization problem (3.5) can be written as:

$$\begin{bmatrix} R_{1,1} & -R_{1,2} \\ \vdots & \vdots \\ R_{N,1} & -R_{N,2} \end{bmatrix} \begin{pmatrix} c_1 \\ c_2 \end{pmatrix} = \begin{pmatrix} d_{1,1} - d_{1,2} \\ \vdots \\ d_{N,1} - d_{N,2} \end{pmatrix} \tag{3.6}$$

This linear least squares problem (3.6) can be solved with SVD. Then, we have optimal c_1, c_2 but they are not unique because they have a null vector due to kinematics. That is, for all the points on the joint axis passing through the joint position, (3.5) is minimized. To deal with this, we assume that the joint positions are on the center line of the index finger. Then, we get the length of each phalanx using the distance between the corresponding joints. However, for DP, we have no information of fingertip position which is difficult to measure due to its compliance, so we use the conventional ratio between MP and DP. This analysis technique is used to measure the human joint angles whose axes are not exactly parallel and positions are difficult to define in appearance [24, 25]. The joint angles are shown in Fig. 3.2.

TABLE 3.1: Length of index finger phalanges

Phalanx	Length (mm)
PP (between MCP and PIP)	$l_{PP} = 44.6$
MP (between PIP and DIP)	$l_{MP} = 25.4$
DP (between DIP and fingertip)*	$l_{DP} = 20.5$

*We use the ratio, $l_{MP}/l_{DP} = 1.24$ [26].

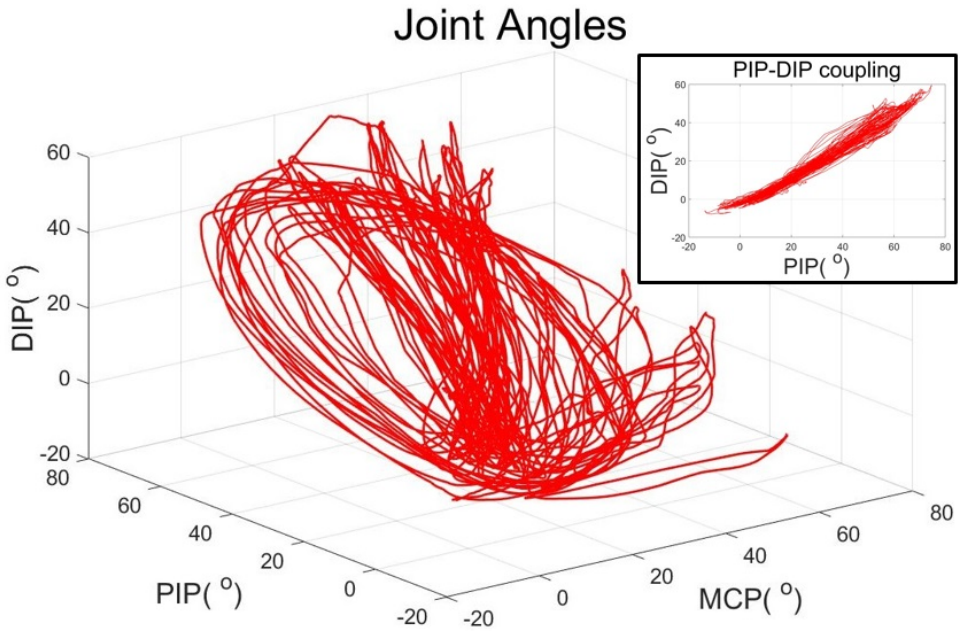

FIGURE 3.2: Joint angles during free motion

3.2.2 PCA for the Joint Space

We can see that the joint angle measurements nearly form a plane in Fig. 3.2. With this result and the knowledge of PIP-DIP coupling, we confirm that we can generate the index finger motions with 2 active tendons. We then apply the principal component analysis (PCA) to find the actuated and the un-actuated directions. Since PCA reduces the dimensionality of a data set and finds the main directions based on its variance [27], we attribute two major directions to the actuated space and the remaining one to the un-actuated space. For the joint angle data $q = [q_{MCP};\ q_{PIP};\ q_{DIP}]$, we calculate its covariance matrix $C \in \Re^{3\times3}$

and apply the eigenvalue decomposition.

$$V = \left[V_a \;\middle|\; V_u \right] = \left[\begin{array}{cc|c} 0.1781 & 0.9839 & -0.0150 \\ 0.7674 & -0.1293 & 0.6280 \\ 0.6159 & -0.1234 & -0.7781 \end{array}\right],$$
$$D = \text{diag}[887.0367,\ 232.6682,\ 7.7405] \tag{3.7}$$

where $V \in \Re^{3\times3}$ is the matrix whose columns are the eigenvectors of the covariance matrix, $V_a \in \Re^{3\times2}$ is the matrix consisting of the first two columns of V, $V_u \in \Re^3$ is the last column of V, and $D \in \Re^{3\times3}$ is the diagonal matrix whose diagonal elements are corresponding eigenvalues.

Among the elements in D, the last eigenvalue 7.7405 is much smaller than the others. That means the actuated space can be approximated as a 2 DoF plane and the corresponding eigenvector V_u is a normal vector of that plane. Since the actuated space is range space of $K^{-1}J_a^T$, this V_u becomes its null vector. On the contrary, V_a is basis of the actuated space and their linear combination is $K^{-1}J_a^T$. Here, we do not use V_a as $K^{-1}J_a^T$ directly because PCA is based on the average and variance of the data set. That is, V_a can vary depending on how the finger moves during the experiments. However, V_u is determined by finger anatomy and almost same for each trial. The results from PCA is presented in Fig. 3.3.

We find the actuated space and the un-actuated space. However, in the quasi-static forced kinematic equation (2.8), the motion is affected by both stiffness

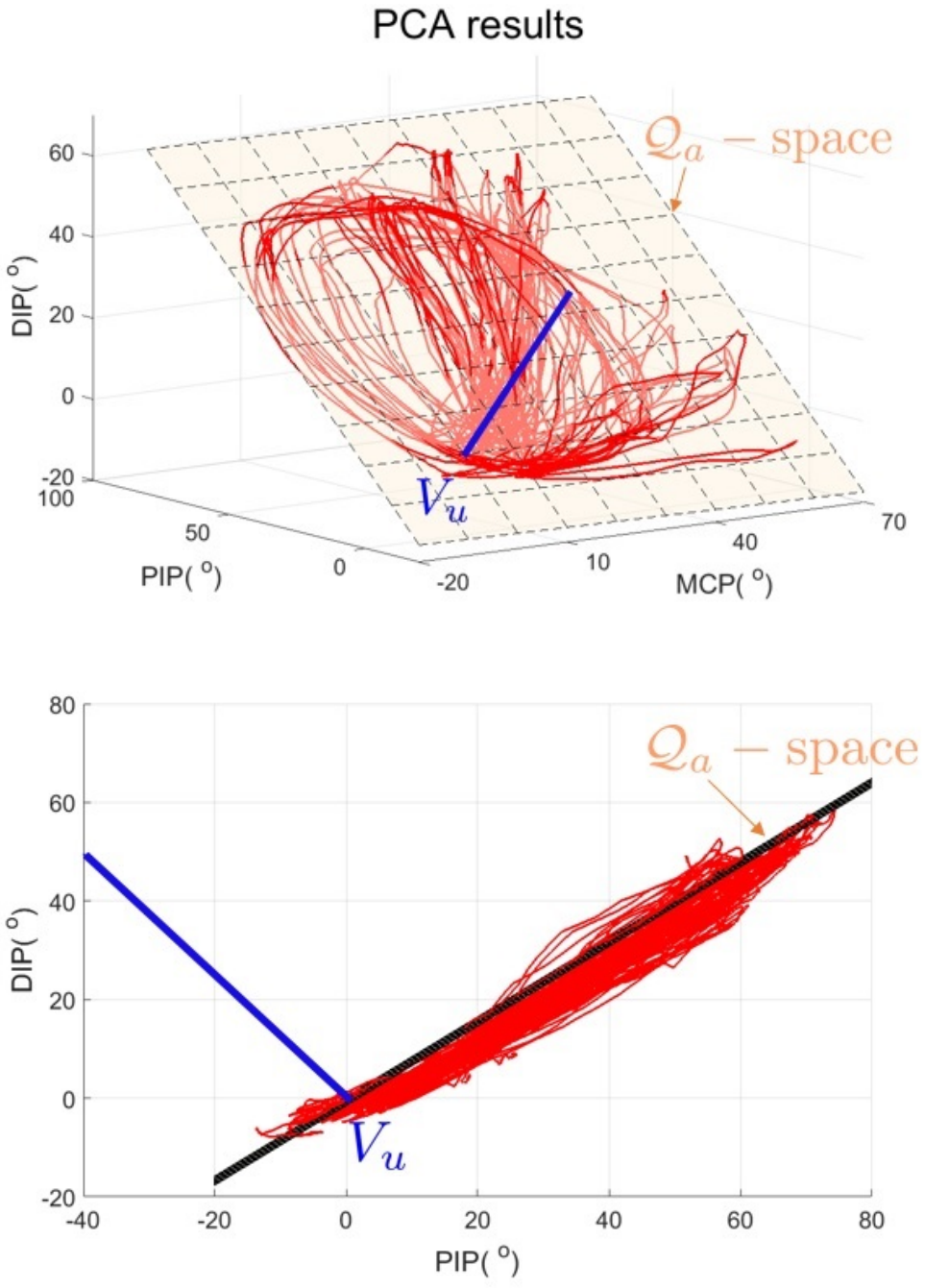

FIGURE 3.3: Joint angle space from PCA

K and active tendon routing J_a, so we can not get exact values of them yet. In the following sections, we introduce additional analysis to determine design parameters: stiffness K, active tendon routing J_a, and initial position q_0.

3.3 Stiffness Design via Un-Actauted Deformation Minimization

We can not control the un-actuated displacement q_u. However, we can maintain the finger configuration while increasing contact force for some pinching pushing postures. That is, for those configurations, there is little un-actuated deflection, and actuation force of muscles and tendons can counteract contact force. Here, we measure joint angles and contact force for those sets. We then find null vector of active tendon routing N_a in (3.1) and the stiffness K to minimize the un-actuated deformation. Of course, we can reduce this un-actuated deformation by enlarging stiffness K, but in (2.7), the motion is generated by $K^{-1}J_a^T\tau_a$, and then large stiffness leads to the need for large actuation. Therefore, we analyze the un-actuated directional stiffness K_u and find the efficient stiffness having human-like motion.

3.3.1 Experimental Settings

We measured joint angles and contact force simultaneously to calculate their effect on the joints and deflection in un-actuated direction. As shown in Fig.

3.4, we used a OptoForce 6-axis F/T sensor (HEX-58-RE-400N) to measure the force exerted on fingertip. We measured 6 pushing postures and for each trial, the subject maintained the posture while increasing contact force as large as possible. The results of the experiments are summarized in Table. 3.2.

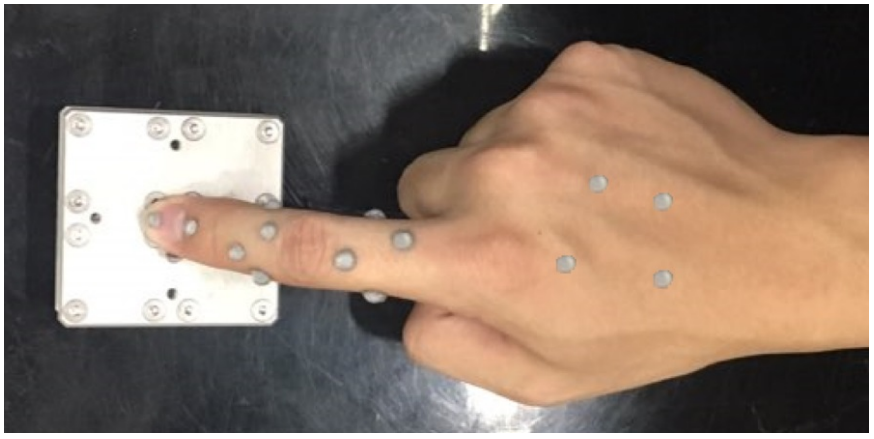

FIGURE 3.4: Experimental settings to measure joint angles and contact force

TABLE 3.2: Joint angles and contact forces during pinching pushing

No.	Joint Angles (°)*	Contact Force (N)**
1	10.70, 46.41, 25.73	5.6229, 0.5006
2	5.50, 17.46, 20.02	6.0186, 0.5093
3	1.31, 32.92, 24.81	6.6124, 0.7607
4	7.87, 55.21, 26.97	5.5702, 1.5177
5	4.64, 45.43, 27.94	6.4579, 1.1187
6	9.59, 51.72, 26.73	7.2287, 1.4127

*The 1st for MCP, the 2nd for PIP, the 3rd for DIP.
**The 1st is normal and the 2nd is along to the plane.

3.3.2 Minimization of the Un-Actuated Deformation

Our design goal is minimizing the un-actuated deformation q_u. This enables the system to be robustly controlled despite the existence of contact force while pushing and grasping. From the stiffness decomposition in Sec. 3.1, we have

$$\begin{aligned} q_u = N_a \xi_u &= N_a K_u^{-1} N_a^T G^T(q) F \\ &= N_a (N_a^T K N_a)^{-1} N_a^T G^T(q) F \end{aligned} \tag{3.8}$$

For N_a which is the null vector of active tendon routing J_a, we have only its direction and can not define its exact size. However, it do not affect the un-actuated deformation q_u, so we regard N_a as a unit vector. Then, minimizing (3.8) is same with minimizing the un-actuated variable $\xi_u \in \Re$.

$$\xi_u = (N_a^T K N_a)^{-1} N_a^T G^T(q) F \tag{3.9}$$

There still remain two unknown variables, N_a and K, but we can find their relationship using V_u in (3.7).

$$\begin{aligned} \left[-K^{-1} J_a^T\right]^T \cdot V_u = -J_a K^{-1} \cdot V_u = 0 \\ K^{-1} V_u = -N_a, \quad K N_a = -V_u \end{aligned} \tag{3.10}$$

With this, we can rewrite (3.9) as:

$$\xi_u = \frac{N_a^T G^T(q) F}{-N_a^T V_u} \tag{3.11}$$

Minimizing (3.11) is maximizing the denominator meaning the un-actuated stiffness K_u and minimizing the numerator meaning the effect of the contact force transmitted to the un-actuated space. Then, we define the optimization problem to find N_a as:

$$\begin{aligned} \text{minimize} \quad & f(N_a) = \sum_{i=1}^{6} |\xi_{u,i}| = \sum_{i=1}^{6} \left| \frac{N_a^T G^T(q_i) F_i}{-N_a^T V_u} \right| \\ \text{subject to} \quad & \|N_a\| = 1 \\ & K_u = -N_a^T V_u \geq 0 \end{aligned} \tag{3.12}$$

where $f(N_a)$ is the absolute sum of $\xi_{u,i}$, the first constraint means N_a is a unit vector, and the second constraint comes from the positive definiteness of the un-actuated stiffness $K_u := N_a^T K N_a$. This inequality also eliminates the opposite directional solution and then, the solution becomes unique. We calculate the contact Jacobian $G(q_i)$ using the phalnages length in Table. 3.1. Using the MATLAB Optimization Toolbox, we get N_a.

$$N_a = \begin{pmatrix} 0.0498 \\ -0.6252 \\ 0.7789 \end{pmatrix} \tag{3.13}$$

3.3.3 Determination of Stiffness

We have not calculated the exact value of the stiffness K and the active tendon routing J_a because they are coupled in the system motion. However, now we have V_u in (3.7) and N_a in (3.13), so we can calculate the stiffness K using their relation (3.10).

$$V_u = -KN_a = -A(N_a)\begin{pmatrix} k_1 \\ k_2 \\ k_3 \\ k_4 \\ k_5 \\ k_6 \end{pmatrix}, \quad K = \begin{bmatrix} k_1 & k_2 & k_3 \\ k_2 & k_4 & k_5 \\ k_3 & k_5 & k_6 \end{bmatrix} \tag{3.14}$$

where $A(N_a) \in \Re^{3\times 6}$ is the matrix whose elements are zero or the elements of the N_a. We assume that the stiffness K is symmetric. Then, we can define this with 6 variables k_i $(i = 1, \cdots, 6)$. The rank of A is 3, so there are 3 independent null vectors. Since we only use 1 DoF V_u and N_a which are related to the un-actuated space to get the 3 DoF stiffness matrix K, the null vectors are related to the actuated space. That is, they do not affect the un-actuated stiffness K_u and the result in Sec. 3.3.2. Also, with these null vectors, we can adjust the stiffness K for certain purpose while satisfying the results of the free motion and the pinch grip experiments. For simplicity, we make the stiffness matrix diagonal. We can produce diagonal stiffness using only torsional springs on joints without using

passive tendons. There are two main advantages from using the torsional spring: its implementation is much easier, and torsional spring works bilaterally (passive tendon needs pre-tension to operate bilaterally).

$$K = \alpha \cdot \text{diag}[0.3011,\ 1.0045,\ 0.9990]N \cdot mm/deg \tag{3.15}$$

There remains scale factor $\alpha \in \Re$ as our analysis is based on the direction and does not consider its size yet. To determine this α, so we have to consider the actuator, actuator pulley radii, and range of motion.

3.4 Active Tendon Routing and Initial Joint Angles Design via Motion Analysis

Our design targets are the stiffness K, active tendon Jacobian J_{θ_a}, and initial configuration q_0 in the quasi-static forced kinematic equation (2.8). In Sec. 3.3.3, we describe how to determine the stiffness K using the un-actuated deformation. Here, we address the problem to find two remaining design parameters: active tendon routing J_a and initial joint angles q_0. For tendon routing, we have to consider its unique characteristics. First, tendons can transmit only positive tensile force. That is, they work unilaterally unlike general motor actuation. Second, the joint pulleys, which tendons go through, should not be too small or too large. This comes from the system size. The joint pulley radii should be larger than

joint radii (lower bound r_{min}) and smaller than the phalanx radii (upper bound r_{max}). Considering these drawbacks, we define the below optimization problem to search efficient active tendon routing and initial configuration.

$$\begin{aligned} \text{minimize} \quad & f(J_{\theta_a},\ q_0) = \max(\tau_{a,1}) + \max(\tau_{a,2}) \\ \text{subject to} \quad & \tau_a(J_{\theta_a}, q_0, q_i) \geq 0, \quad i = 1, \cdots, N \\ & J_{\theta_a} \cdot N_a = 0 \\ & (q_0 - \bar{q})^T \cdot V_u = 0 \\ & r_{\min} \leq (J_{\theta_a})_{i,j} \leq r_{\max} \ \text{ or } \ (J_{\theta_a})_{i,j} = 0 \end{aligned} \tag{3.16}$$

where $\tau_{a,1},\ \tau_{a,2} \in \Re$ are the input torque of the 1st and 2nd actuators, and $q_i,\ \bar{q} \in \Re^3$ is the i-th and the average joint angle data from the free motion experiments (Fig. 3.2). The object function $f(J_{\theta_a},\ q_0)$ is the sum of maximum actuator torque to generate the joint angles. Then, with the optimal design parameters, we can cover the free motion with minimal actuation inputs. The first constraint means that optimized variables should be able to generate the free motion joint angles q_i in Fig. 3.2 with positive actuation inputs. As stated before, this comes from the unilaterality of tendon routing. Since the number of raw data is 66307, we also extract data in one out of 100 to reduce calculation time and the number of data is reduced to 664. Then, we have 664 inequality constraints for positiveness of the actuation input τ_a. We can derive these $\tau_{a,1}, \tau_{a,2}$ using (2.8).

$$\tau_a = (-K^{-1} J_{\theta_a}^T R_{\theta_a}^{-1})^{\dagger} (q - q_0)$$

We assume that two actuation pulley radii, which are diagonal elements of R_{θ_a} are same and constant, so they do not affect the solution and they can be determined with the consideration of the actuation. This assumption is also applied when calculating the object function $f(J_{\theta_a},\ q_0)$. The second constraint, $J_a \cdot N_a = 0$, comes from the definition of N_a which is the null vector of the active tendon routing J_a. Since we assume that the actuator pulley radii $r_{\theta_{a1}}, r_{\theta_{a2}}$ are same, N_a should also be the null vector of J_{θ_a}. The third constraint ensures that the q_0 be on the plane of PCA. The PCA uses the covariance of data, so our joint angle plane in Fig. 3.3 is lying on the mean value $\bar{q}$ and this kinematic relation can be formulated as equality constraint. The last two equations represent the range of pulley radii. They should be within the bound or zero. The zero element means the corresponding tendon does not pass that joint. We adopt $r_{\min}$ as $3mm$ and $r_{\max}$ as $5mm$ with the consideration of our system design. These bound can vary with how to design the system, and then it results in different tendon routing. Since this constraint is not continuous and hard to solve, we distribute zeros to the arbitrary pulleys and use only the range of pulley radii constraint for the others. For some trials, we change the pulleys with zero size and compare the value of the objective function f. Since the optimization problem (3.16) is still highly complex and nonlinear, we use the MATLAB Optimization Toolbox.

The results are shown in (3.17) and Fig. 3.5. There appears scale factor $\beta \in \Re$ due to the stiffness scale factor α in (3.15) and actuation pulley radii R_a. With the consideration of the actuator input, we can determine both α and β to implement the UATD robotic finger having similar performance with human hand.

$$q_0 = \begin{pmatrix} -15.3080 \\ -6.0744 \\ -8.9958 \end{pmatrix}^o, \; J_{\theta_a} = \begin{bmatrix} -5 & 3.3549 & 3.0127 \\ 0 & -5 & -4.0134 \end{bmatrix} mm,$$

$$-K^{-1}J_a^T = -K^{-1}J_{\theta_a}^T R_{\theta_a}^{-1} = \begin{bmatrix} v_1 & v_2 \end{bmatrix} = \beta \begin{bmatrix} 16.6058 & 0 \\ -3.3398 & 4.9776 \\ -3.0156 & 4.0174 \end{bmatrix} \tag{3.17}$$

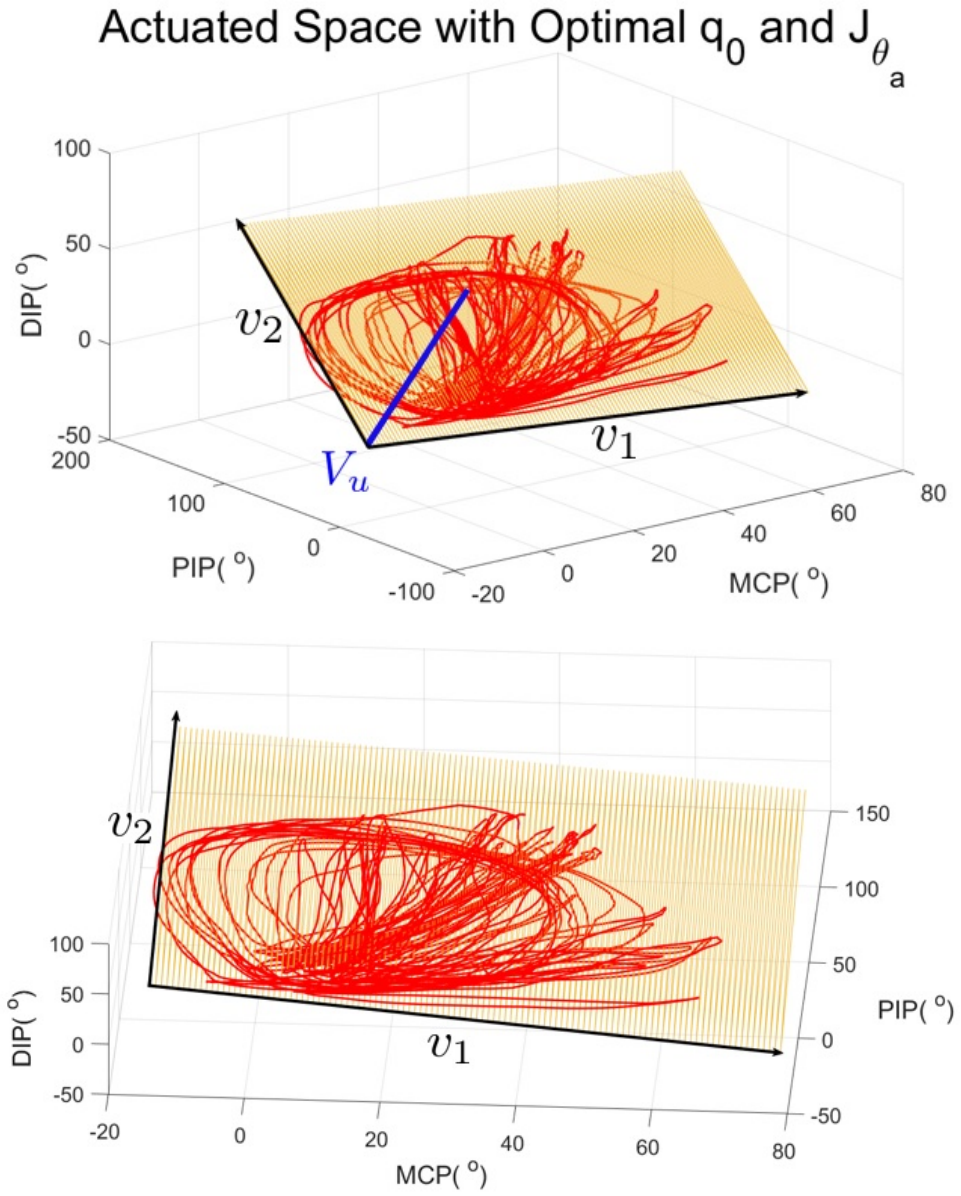

FIGURE 3.5: Actuated Space with the optimal design parameters: initial joint angles q_0 and active directions v_1, v_2

Chapter 4

Control and Simulation Results

4.1 Control

In this section, we propose a simple PD-based control to track desired finger configuration during both free motion and contact. Since the proposed UATD robotic finger is under-actuated, we can not perfectly generate arbitrary desired joint angles $q_d \in \Re^3$. Therefore, here, we restrict the desired joint angle $q_d \in \Re^3$ to the actuated space $\mathcal{Q}_a$, which is the free motion plane in Fig. 3.3. That is, we

can generate this q_d with $q_{a,d}$ which is generatable with our control input τ_a.

$$q_d = q_0 + q_{a,d}$$

We then aim to track $q_{a,d}$ which is the component of q_d in the actuated space $\mathcal{Q}_a$. we design a control to make q_a go to $q_{a,d}$. It is natural to select θ_a as a control variable because this is directly related to the actuated space and physically means the actuator angle. With the tendon kinematics, the desired actuator angle $\theta_{a,d}$ is defined as:

$$\theta_{a,d} = -J_a(q_d - q_0) = -J_a q_{a,d}$$

Then, from the decomposed quasi-static equation (3.4), we design the following control using this $\theta_{a,d}$.

$$\begin{aligned}\tau_a =& K_m(\theta_{a,d} - \theta_a) + K_a\theta_{a,d} + D_m(\dot{\theta}_{a,d} - \dot{\theta}_a) \\ &+ K_a J_a K^{-1} G^T(q) F\end{aligned} \tag{4.1}$$

where $K_m, D_m \in \Re^{2\times 2}$ are the gain matrix. The second term in the right hand side, $K_a\theta_{a,d}$, is needed to compensate the restoring force from the system stiffness K. The last term is cancellation of the contact force on the actuated space. If we have the force measurements, we can calculate this term with joint angle q and

contact force F. Then, we have

$$(K_m + K_a)e_{\theta_a} + D_m\dot{e}_{\theta_a} = 0$$

where e_{θ_a} is defined as $\theta_a - \theta_{a,d}$. From this error dynamics, the error e_{θ_a} goes to 0 for constant $\theta_{a,d}$. Although we neglect the dynamics effects, our control works well as those effects are relatively small.

With the control law in (4.1), we can perfectly generate the deisred joint angle $q_d \in \mathcal{Q}_a$ during the free motion where the contact force F is zero. However, if there is contact, it incurs the un-actuated deformation q_u and the error for q_d converges to

$$e_q = q_u = N_a K_u^{-1} N_a^T G^T(q) F$$

which we can not eliminate due to the under-actuation.

4.2 Simulation Results

We use our design parameters and the mass calculated using the density of human body [28]. Also, we define the scale factor α in (3.15) as 0.7232 and the actuator pulley radii R_{θ_a} as $11mm$. Then, we first check the convergency of the proposed control in (4.1) for the constant desired joint angle q_d. Fig. 4.1 shows the joint angle errors and the actuator angle errors go to zero. The un-actuated deformation ξ_u also goes to zero due to the natural damping.

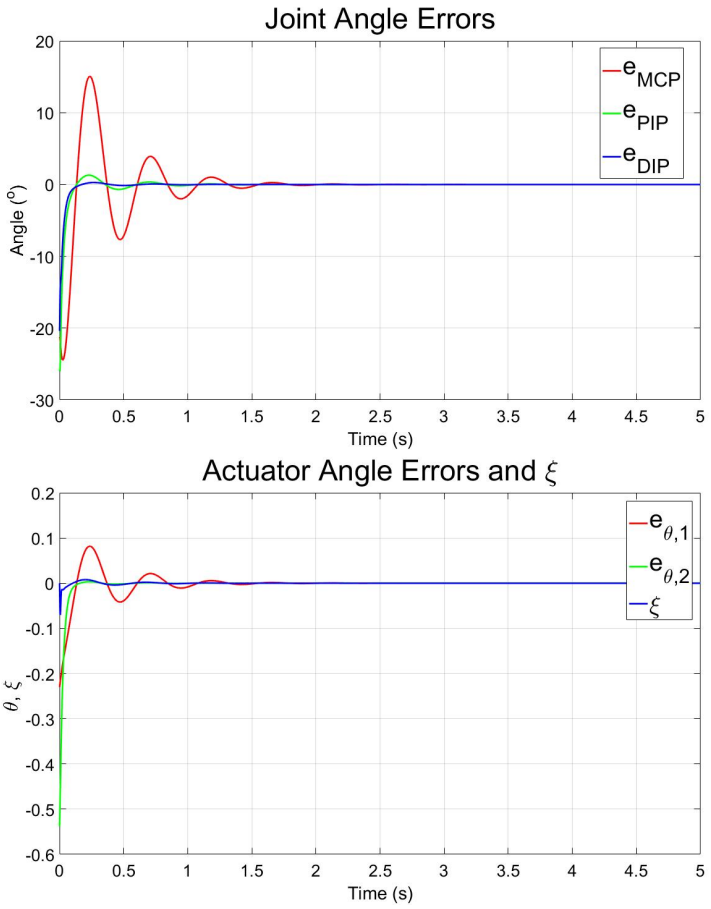

FIGURE 4.1: Joint angle errors, actuator angle errors and un-actuated deformation under the proposed PD control

Second, we apply the contact force in Table. 3.2 to our system model and verify the un-actuated deformation ξ_u. The reults are presented in Fig. 4.2. With our design parameters, the maximum magnitude of the un-actuated deformation is 2.9158°.

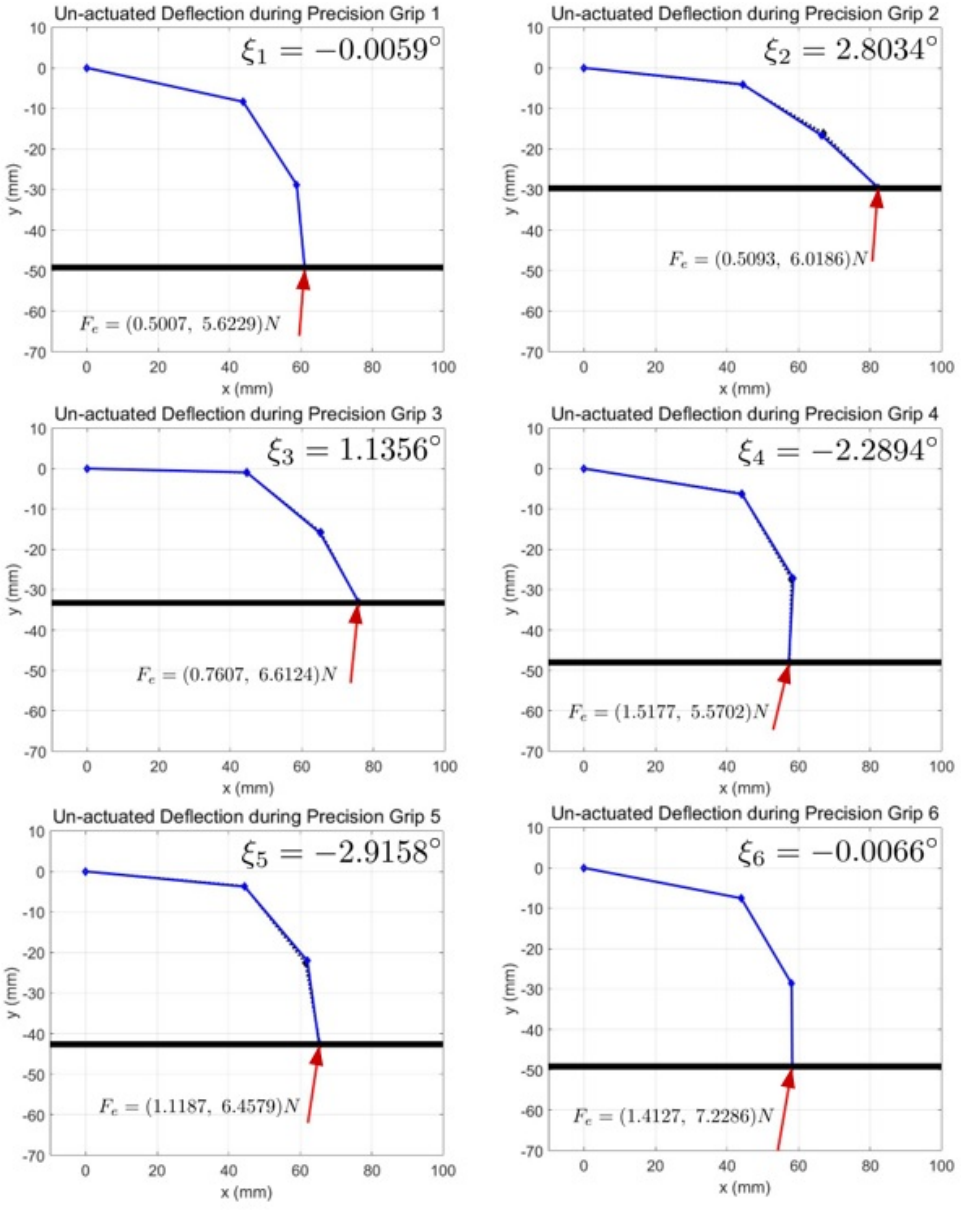

FIGURE 4.2: Finger posture before and after exerting force on fingertip (Dashed line : before, Blue line : after)

Chapter 5

Conclusion and Future Work

5.1 Conclusion

In this paper, we presented a novel design framework for the UATD robotic finger. We decomposed the system equation based on its stiffness. We then defined the actuated space generated by actuations and the un-actuated space from under-actuation. Before finding design parameters, we measured the free motion to define both space and we conclude that only two actuation is enough to generate the free motion of the index finger motion due to the joint coupling between PIP and DIP joints. Also, we measured the joint angles and force during the contact with large force and investigated the stiffness to minimize the un-actuated deformation. We showed that there is design freedom in stiffness and utilized that

to make stiffness be diagonal. With this stiffness, we found the optimal active tendon routing and initial configuration to generate the free motion under the system constraints: 1) joint pulley range from system size; and 2) unilaterality of tendon tensile force. Lastly, we designed a PD-based control to track the desired joint angle and show the simulation results.

To our knowledge, there are no systematic design frameworks for designing the UATD robotic finger while taking into account both the free motion and the contact, so we believe the framework proposed here is the very first result along this line of research. Also, this UATD finger can be utilized as the component of UATD robotic hand for more complex tasks (e.g., grasping, in-hand manipulation, etc.)

5.2 Future Work

Future work includes the implementation of proposed UATD robotic finger. To do that, we have to study the optimal actuator pulley radii and choose proper actuators with the consideration of tasks. And then, we plan to develop this UATD robotic finger into the UATD robotic hand to mimic the human hand. In my thesis, we used the human phalanx for link length. Future work also investigate the optimiztion method to determine the link length for given tasks.

Bibliography

[1] S. Jacobsen, E. Iversen, D. Knutti, R. Johnson, and K. Biggers, "Design of the Utah/MIT dextrous hand," In *Proceedings of IEEE International Conference on Robotics and Automation*, pp. 1520-1532, 1986.

[2] J. K. Salisbury and J. J. Craig, "Articulated hands: Force control and kinematic issues," *International Journal of Robotics Research*, vol. 1, no. 1, pp. 4-17, 1982.

[3] B. M. Jau, "Dexterous telemanipulation with four fingered hand system," In *Proceedings of IEEE Conference on Robotics and Automation*, pp. 338-343, 1995.

[4] R. O. Ambrose, H. Aldridge, R. S. Askew, R. R. Burridge, W. Bluethmann, M. Diftler, C. Lovchik, D. Magruder, and F. Rehnmark, "Robonaut: Nasa's space humanoid," *IEEE Intelligent Systems and Their Applications*, vol. 15, no. 4, pp. 57-63, 2000.

[5] M. Grebenstein, A. Albu-Schffer, T. Bahls, M. Chalon, O. Eiberger, W.Friedl, R. Gruber, U. Hagn, R. Haslinger, and H. Hoppner, "The DLR hand arm system," In *Proceedings of IEEE Internation Conference on Robotics and Automation*, pp. 3175-3182, 2011.

[6] Shadow Dexterous Hand, Shadow Robot Company. (May 15, 2012). [Online]. Available: http://www.shadowrobot.com/hand.

[7] Z. Xu and E. Todorov, "Design of a highly biomimetic anthropomorphic robotic hand towards artificial limb regeneration," In *IEEE International Conference on Robotics and Automation*, pp. 3485-3492, 2016.

[8] E. Nazma and S. Mohd, "Tendon driven robotic hands: A review," *International Journal of Mechanical Engineering and Robotics Research*, vol. 1, no. 3, pp. 350-357, 2012.

[9] K. J. Van-Zwieten, K. P. Schmidet, G. J. Bex, P. L. Lippens, and W. Duyvendak, "An analytical expression for DIP-PIP flexion interdependence in human fingers," *Acta of Bioengineering and Biomechanics*, vol. 17, no. 1, pp. 129-135, 2015.

[10] R. Ozawa, K. Hashirii, Y. Yoshimura, M. Moriya, and H. Kobayashi. "Design and control of a three-fingered tendon-driven robotic hand with active and passive tendons," *Autonomous Robots*, vol. 36, no. 1, pp. 67-78, 2014.

[11] R. Ozawa, H. Kobayashi, and K.Hashirii, "Analysis, classification, and design of tendon-driven mechanisms," *IEEE Transactions on Robotics*, vol. 30, no. 2, pp. 396-410, 2014.

[12] J. M. Inouye, J. J. Kutch, and F. J. Valero-Cuevas, "A novel synthesis of computational approaches enables optimization of grasp quality of tendon-driven hands," *IEEE Transactions on Robotics*, vol. 28, no. 4, pp. 958-955, 2012.

[13] J. M. Inouye and F. J. Valero-Cuevas, "Anthropomorphic tendon-driven robotic hands can exceed human grasping capabilities following optimization" *International Journal of Robotics Research*, vol. 33. no. 5, pp. 694-705, 2014.

[14] J. M. Inouye and F. J. Valero-Cuevas, "Computational optimization and experimental evaluation of grasp quality for tendon-driven hands subject to design constraints," *Journal of Mechanical Design*, vol. 136, no. 2, 2014.

[15] L. Zollo, S.Roccella, E. Guglielmelli, M. C. Carrozza, and P. Dario, "Biomechatronic design and control of an anthropomorphic artificial hand for prosthetic and robotic applications," *IEEE/ASME Transactions on Mechatronics*, vol. 12, no. 4, pp. 418-429, 2007.

[16] C. Y. Brown and H. H. Asada, "Inter-finger coordination and postural synergies in robot hands via mechanical implementation of principal component analysis," *IEEE/RSJ International Conference on Intelligent Robots and Systems*, pp. 2877-2882, 2007.

[17] M. G. Catalano, G. Grioli, E. Farnioli, A. Serio, C. Piazza, and A. Bicchi, "Adaptive synergies for the design and control of the Pisa/IIT SoftHand," *International Journal of Robotics Research*, vol. 33, no. 5, pp. 768-782, 2014.

[18] G. Palli, C. Melchiorri, G. Vassura, U. Scarcia, L. Moriello, G. Berselli, A. Cavallo, G. De Maria, C. Natale, S. Pirozzi, C. May, F. Ficuciello, and B. Siciliano "The DEXMART hand: Mechatronic design and experimental evaluation of synergy-based control for human-like grasping," *International Journal of Robotics Research*, vol. 33, no. 5, pp.799-824, 2014.

[19] J. N. A. L. Leijnse, P. M. Quesada, and C. W. Spoor, "Kinematic evaluation of the finger's interphalangeal joints coupling mechanism-variability, flexion-extension differences, triggers, locking swanneck deformities, anthropometric correlations," *Journal of Biomechanics*, vol. 43, no. 12, pp. 2381-2393, 2010.

[20] J. Lin, Y. Wu, and T. S. Huang, "Modeling the constraints of human hand motion," In *Proceedings of IEEE Workshop on Human Motion*, pp. 121-126, 2000.

[21] L. Hoyet, K. Ryall, R. Mcdonnell, and C. O'Sullivan, "Sleight of hand: perception of finger motion from reduced marker sets," In *Proceedings of the ACM SIGGRAPH Symposium on Interactive 3D Graphics and Games*, pp. 79-86, 2012.

[22] X. Zhang, S. W. Lee, and P. Braido, "Determining finger segmental centers of rotation in flexion–extension based on surface marker measurement," *Journal of Biomechanics*, vol. 36, no. 8, pp. 1097-1102, 2003.

[23] R. M. Ehrig, W. R. Taylor, G. N. Duda, and M. O. Hellor, "A survey of formal methods for determining functional joint axes," *Journal of Biomechanics*, vol. 40, no. 10, pp. 2150-2157, 2007.

[24] O. Warlow and S. Lawson, "A tehchnique for motion capture of the finger using functional joint centres and the effect of calibrration range of motion on its accuracy," In *Proceedings of the Institution of Mechanical Engineers, Part H: Journal of Engineering in Medicine*, vol. 226, no. 5, pp. 360-367, 2012.

[25] O. Warlow, "Kinematic and anatomical measurement for biomechanical finger models," Ph.D. Thesis, 2012.

[26] R. Hamilton and R. A. Dunsmuir, "Radiographic assessment of the relative lengths of the bones of the fingers of the human hand," *Journal of Hand Surgery (British and European Volume)*, vol. 27, no. 6, pp. 546-548, 2002.

[27] I. T. Jolliffe, *Principal component analysis.* John Wiley & Sons, Ltd, 2002.

[28] H. J. Krzywicki and K. S. Chinn, "Human body density and fat of an adult male population as measured by water displcement," *The American Journal of Clinical Nutrition*, vol. 20, no. 4, pp. 305-310, 1967.

요약

본 논문에서는 부족구동 텐던구동 로봇 손 디자인을 위한 새로운 방법론에 대해서 기술한다. 먼저, 강성 기반 시스템 방정식 분할을 통해 구동공간과 비구동공간으로 나누었다. 구동공간은 외력이 작용하지 않는 자유운동이 나타나는 반면, 비구동공간은 접촉이 있을 때 변형으로 나타난다. 자유운동과 접촉 시의 사람의 검지 손가락 관절각과 접촉력 측정 결과를 토대로 시스템 제약 조건(손가락 두께, 텐던 장력의 단방향성) 하에서 사람 손 움직임을 모사하기 위한 설계 변수(강성, 텐던 라우팅, 초기 자세)를 찾기 위한 최적화 문제를 정의하고 해를 구하였다. 이후, 관절각 추종을 위한 PD 제어기를 설계하고, 시뮬레이션을 통해 검증하였다.

주요어: Under-actuated tendon-driven robotic finger, Stiffness decomposition
학번: *2014-21870*